Solid State Ionics 296 (2016) 78–84

Contents lists available at ScienceDirect

Solid State Ionics

journal homepage: www.elsevier.com/locate/ssi

Transmission electron microscopy of topochemical conversion interface between $La_2Ti_2O_7$ reactive template and perovskite product $Li_{0.16}La_{0.62}TiO_3$ electrolyte

Aslihan Orum [a], Melike Mercan Yildizhan [b], Meltem Sezen [c], Mehmet Ali Gulgun [b,c], Kazumasa Takatori [d], Hiroaki Kadoura [d], Masamichi Yoshimura [a], Toshihiko Tani [a,d,*]

[a] Toyota Technological Institute, Nagoya 468-8511, Japan
[b] Sabanci University, Faculty of Engineering and Natural Sciences, Istanbul 34956, Turkey
[c] Sabanci University Nanotechnology Application Center, Istanbul 34956, Turkey
[d] Toyota Central Research and Development Laboratories, Inc., Nagakute 480-1192, Japan

ARTICLE INFO

Article history:
Received 13 June 2016
Received in revised form 4 September 2016
Accepted 5 September 2016
Available online 11 September 2016

Keywords:
Topochemical conversion
$(La,Li)TiO_3$ electrolyte
TEM
Interface

ABSTRACT

The topochemical conversion interface between a layered perovskite $La_2Ti_2O_7$ and an ordered regular perovskite $Li_{0.16}La_{0.62}TiO_3$, (LLTO) electrolyte was investigated using high-resolution transmission electron microscopy and scanning-transmission electron microscopy (STEM) for platelike $La_2Ti_2O_7$ particles semi-reacted (at 1273 K) with the complementary reactants $Li_4Ti_5O_{12}$ and TiO_2. High-temperature X-ray diffraction analysis confirmed that regular perovskite-type product was formed in situ at 1173 K and above without the formation of any intermediate phases. The crystallographic relationship between the product and the template at the interface was determined by selected area electron diffraction to be orthorhombic LLTO [001](110) || monoclinic $La_2Ti_2O_7$ [001](100). STEM revealed that the alternating La-rich and La-poor planes in the LLTO phase were aligned perpendicular to the interface, which was parallel to the interlayers, i.e., the (200) planes of the $La_2Ti_2O_7$ template. At the interface, a unit-cell-thick $La_2Ti_2O_7$ or a block of four-layered TiO_6 octahedra between two interlayers is a basic unit converted into a regular perovskite-type product by shifting the block with La along the *c*-axis. This microscopic observation of the interface suggests the possibility of designing domain structures with improved ionic conductivity.

1. Introduction

Lithium ion batteries (LIBs) are widely used in electrical vehicles and portable devices, due to their high energy density [1]. Current LIBs on the market use a liquid electrolyte that consists of a Li salt dissolved in a liquid organic solvent [1]. However, liquid electrolytes are potentially hazardous [1,2], which has prompted researchers to develop an alternative electrolyte material for LIBs. One complex oxide, lithium lanthanum titanate ($Li_{3x}La_{2/3-x}TiO_3$) (LLTO), has attracted much attention in many studies for solid-state battery applications, owing to its mechanical and thermal stability over a wide temperature range. These properties enable the production of all-solid-state batteries [3]. The ionic conductivity of polycrystalline LLTO ceramics has both intragranular and boundary components. The intragranular conductivity refers to the conductivity of single crystalline grains ($\sim 10^{-3}$ S·cm^{-1}), while the boundary conductivity, i.e., the contributions from grain boundaries and/or the domain boundaries, is $\sim 10^{-4}$ S·cm^{-1} or less [4,5]. The low boundary conductivity dominates the total ionic conductivity of the ceramics. A possible approach to enhancing the overall ionic conductivity would be to minimize the boundary area and to reduce the negative effects of the boundaries.

LLTO has a pseudocubic perovskite ABO_3-type structure, in which lanthanum atoms exist at A-sites with some vacant positions for lithium atoms [6]. These A-site vacancies are partitioned into La-rich and La-poor planes, which alternate along the ⟨001⟩ direction (⟨100⟩ in pseudocubic notation) for both tetragonal (Li-rich composition; $0.1 \le x < 0.167$) and orthorhombic LLTO (Li-poor composition; $0.03 \le x < 0.1$) [6,7]. The structure of orthorhombic LLTO is illustrated in Fig. 1(b) [8]. Inaguma et al. reported that the La occupancy at A-sites is 0.939 and 0.301 in La-rich and La-poor planes, respectively, for $Li_{0.16}La_{0.62}TiO_3$ [9]. Yashima et al. elucidated that lithium ions and A-site vacancies only exist in the La-poor planes of $Li_{0.16}La_{0.62}TiO_3$, therefore the (002) plane is responsible for ionic conduction [10]. Since La-rich planes effectively act as barriers for Li-ion mobility along the

* Corresponding author at: Toyota Central Research and Development Laboratories, Inc., Nagakute, Aichi, 480-1192, Japan.
E-mail address: toshit@mosk.tytlabs.co.jp (T. Tani).

http://dx.doi.org/10.1016/j.ssi.2016.09.008
0167-2738/

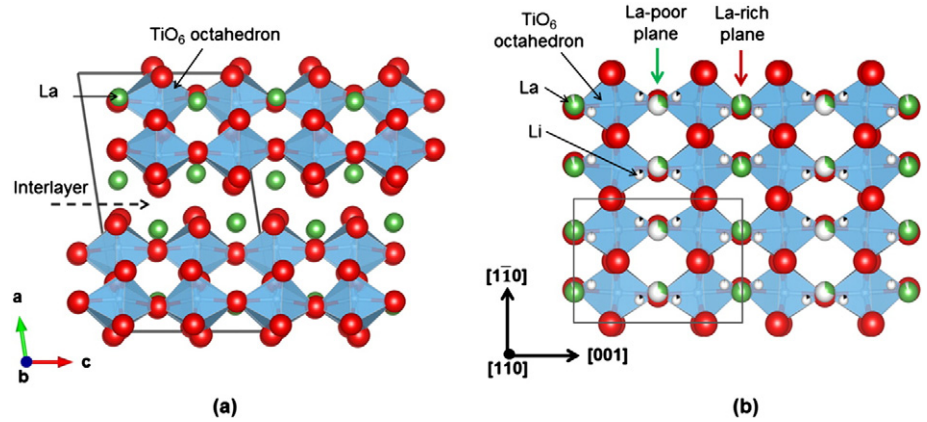

Fig. 1. Crystallographic relationship between (a) $\{110\}_{pc}$-type layered perovskite $La_2Ti_2O_7$ and (b) ordered regular perovskite LLTO [8,14].

[001] direction, two-dimensional Li-ion mobility takes place within the orthorhombic crystal [10]. HRTEM studies revealed that multi-domain structures were formed in polycrystalline LLTO sintered above 1400 K [11,12]. Furthermore, recent studies revealed that orthorhombic LLTO has 90° domain boundaries that influence the ionic migration of lithium during conduction [11,13]. First principles calculations by Moriwake et al. on model domain structures showed that theoretically, an LLTO phase with a single-domain structure would exhibit high Li-ion conduction [13]. In consideration of the structure and conduction mechanism of LLTO, it should have anisotropic or orientation-dependent properties in a single-domain crystal despite having a pseudo-isotropic crystal structure.

Takatori et al. suggested that the orientation of both the crystal lattice and the domain/grain boundaries is important for obtaining an LLTO ceramic with an ionic conductivity as high as that for a single crystal [14]. In this regard, they proposed the preparation of textured LLTO ceramics with a preferred $\{110\}_{pc}$-orientation ("*pc*" denotes pseudocubic notation) by utilizing the reactive-templated grain growth (RTGG) method [14]. In RTGG, a reactive template, which is an anisometric single crystal particle, is used as a seed for a topochemical conversion reaction [15]. Crystallographic and compositional similarity between the reactive template and the target product is necessary in order to form a textured ceramic with the desired composition and to preserve the orientation of the corner-sharing oxygen octahedra during the topochemical reaction [15]. Takatori et al. selected a 110-type layered perovskite, $La_2Ti_2O_7$, in which the interlayers are parallel to the $\{110\}_{pc}$ planes in the perovskite unit cell (Fig. 1(a)), as a reactive template to obtain regular perovskite LLTO ceramics with a preferred $\{110\}_{pc}$ orientation. The layered perovskite $La_2Ti_2O_7$ has a monoclinic structure ($a = 13.015$ Å, $b = 5.546$ Å, $c = 7.817$ Å, $\beta = 98.64°$ [16]). Four corner-sharing TiO_6 octahedra are positioned between two interlayers in the unit-cell. Takatori et al. reported a crystallographic relationship between $La_2Ti_2O_7$ and LLTO in which the *b*-*c* planes of $La_2Ti_2O_7$ are parallel to $\{110\}_{pc}$ in LLTO whereas the *b*- and *c*-axes of $La_2Ti_2O_7$ correspond to the $\langle 110\rangle_{pc}$ and $\langle 100\rangle_{pc}$ directions in LLTO, respectively (Fig. 1) [14,17,18]. However, they did not clarify the conversion of the (110)-type layered perovskite $La_2Ti_2O_7$ into a regular perovskite LLTO microscopically. In fact, no observations have been reported on the reaction interface during the formation of LLTO through topochemical conversion. Microscopic investigation of the reaction interface between $La_2Ti_2O_7$ and LLTO is necessary 1) to confirm the succession of texture without the formation of disturbing intermediate phases [19], 2) to understand how the crystallographic relationship is preserved between the $La_2Ti_2O_7$ reactive template and the LLTO product at the reaction interface, and 3) to observe how an ordered structure is developed in the LLTO product.

There have been several microscopic investigations of topochemical conversion from a layered perovskite into a regular perovskite. A study involving transmission electron microscopy (TEM) carried out on RTGG-processed, $\{100\}_{pc}$-textured $Bi_{0.5}(Na,K)_{0.5}TiO_3$ (BNKT) showed that the regular perovskite-type product BNKT started to form in the vicinity of the surface of a 100-type bismuth-layered perovskite $Bi_4Ti_3O_{12}$ template, preserving the $\langle 100\rangle_{pc}$ orientation [20]. The diffusion of Na and K atoms from complementary reactants into the reactive template during heat treatment induced a change in the crystal structure of the $Bi_4Ti_3O_{12}$ template. The in situ formation of the regular perovskite product was concluded to be topochemical by electron diffraction analysis [20]. In another work by Watanabe et al., the transformation of Aurivillius-phase $Bi_{2.5}Na_{3.5}Nb_5O_{18}$ (BiNN5) into $NaNbO_3$ via topochemical conversion reaction was investigated by TEM [21]. They observed the out-diffusion of Bi ions through the BiNN5 structure during the formation of $NaNbO_3$, while the alignment of the NbO_6 octahedra in BiNN5 was preserved [21].

In the present study, we examine the formation mechanism for an RTGG-processed LLTO ceramic from the 110-type layered perovskite $La_2Ti_2O_7$ through microscopy. TEM analysis was carried out on a semi-reacted specimen to observe the formation of the ordered structure of the LLTO phase at the surface of the $La_2Ti_2O_7$ reactive template. The crystallographic relationship between the template and the target product was investigated to discuss the transformation of the template into the target product. The composition $Li_{0.16}La_{0.62}TiO_3$ was selected for this study since this Li-poor LLTO composition exhibits an ordered structure that is easily detectable by TEM.

2. Experimental

2.1. Preparation of semi-reacted specimen for TEM analysis

Rectangular-platelike $La_2Ti_2O_7$ particles, in which the developed plane was determined to be (200), were prepared by a molten flux method in KCl at 1473 K for 4 h [18] and used as reactive templates for LLTO. The template particles were mixed with complementary reactants, TiO_2 (Tipaque A-100, 99.2%) and $Li_4Ti_5O_{12}$ (Ishihara Sangyo Kaisha, 99.5%), together with an organic solvent premix solution, by ball milling to make a slurry for tape casting. A sheet with a composition in which the La source consisted entirely of the template particles was prepared by tape casting for easy observation of the conversion reaction on the templates. The reaction scheme for the $Li_{0.16}La_{0.62}TiO_3$ composition is:

$$0.31\ La_2Ti_2O_7 + 0.04\ Li_4Ti_5O_{12} + 0.18\ TiO_2 \rightarrow Li_{0.16}La_{0.62}TiO_3.$$

The sheets were stacked and dewaxed at 773 K according to the process route reported by Takatori et al. [14] and the dewaxed bodies were characterized as described below in Section 2.2.

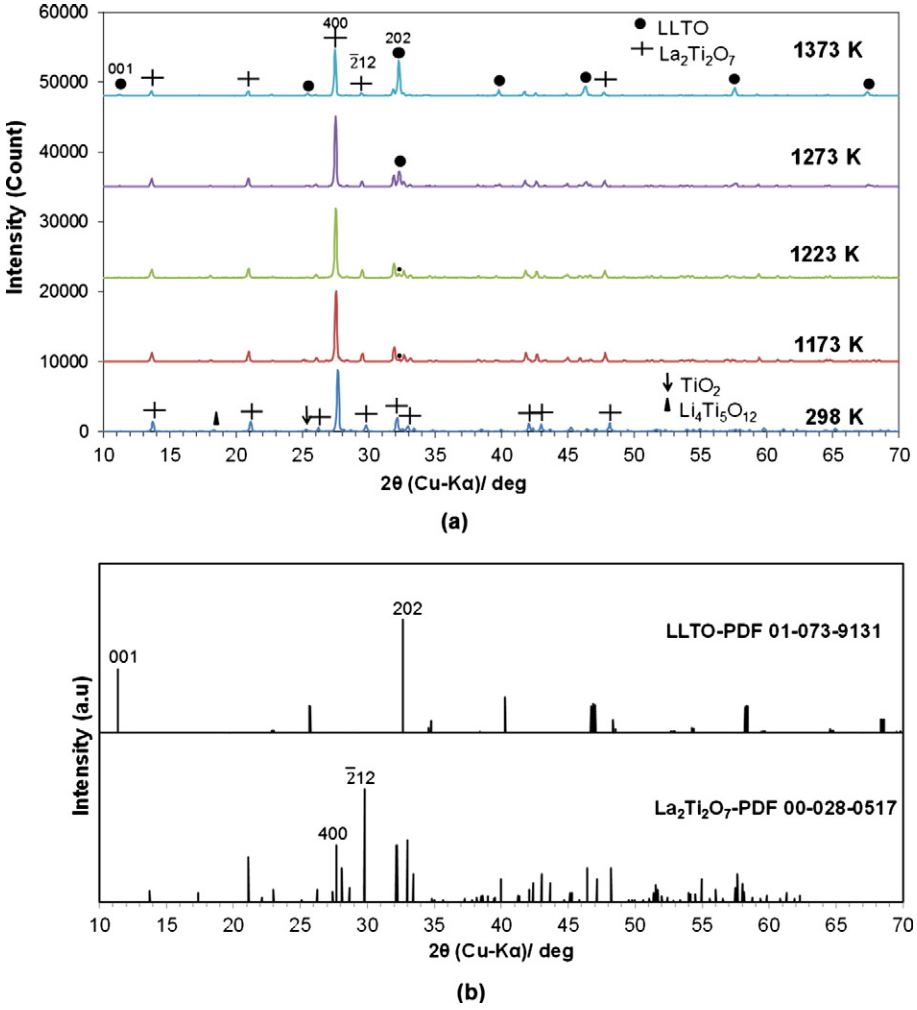

Fig. 2. (a) HTXRD patterns of a dewaxed specimen at 298 K and 1173–1373 K. The XRD patterns were obtained from the surface of a dewaxed body parallel to the tape-casting plane. (b) The ICDD profiles of the $La_2Ti_2O_7$ reactive template and the LLTO product.

2.2. Characterization

To determine the incipient stage of the phase transition from $La_2Ti_2O_7$ to LLTO high-temperature X-ray diffraction (HTXRD; Rigaku Co. RINT TTR II, Cu-Kα) analysis was carried out on the surface of a dewaxed body parallel to the tape-casting plane. The HTXRD analysis was conducted at a heating rate of 20 $K \cdot min^{-1}$ from room temperature to 1073–1573 K. XRD patterns were obtained at a scan speed of 4° min^{-1}, with $2\theta = 10–70°$. The phases present in the specimen were identified based on ICDD data for monoclinic $La_2Ti_2O_7$ [16] and orthorhombic LLTO [22]. After phase identification, specific temperatures (1173 K and 1273 K) were selected for 15-min heat treatment of dewaxed bodies to observe the microstructural changes on the surfaces of the reactive templates. Fracture surfaces of the heat-treated specimens were observed by scanning electron microscopy (SEM; Hitachi SU3500 and Zeiss 1530 Gemini LEO).

A cross-sectional TEM specimen was prepared from a heat-treated specimen (at 1273 K for 15 min) using focused ion beam milling (FIB; JEOL JIB-4501 Multi-Beam FIB-SEM). Two-phase boundary regions consisting of the template and product were selected by SEM and sectioned by FIB. High-resolution TEM (HRTEM) and scanning transmission electron microscopy (STEM) were performed with a JEOL-ARM 200 CFEG operating at 200 kV with a resolution better than 1 Å in STEM imaging mode. High-resolution imaging was conducted with high-angle-annular dark field (HAADF), annular-dark field (ADF), and (annular) bright field ((A)BF) imaging detectors. Selected area electron diffraction (SAED) patterns were obtained from the two-phase boundaries. All energy-dispersive X-ray spectroscopy (EDS) analysis were conducted in STEM-mode using the HAADF detector. The BF-detector was retracted to allow simultaneous EELS measurements of the specimen thickness. The specimen was tilted for measurements to a

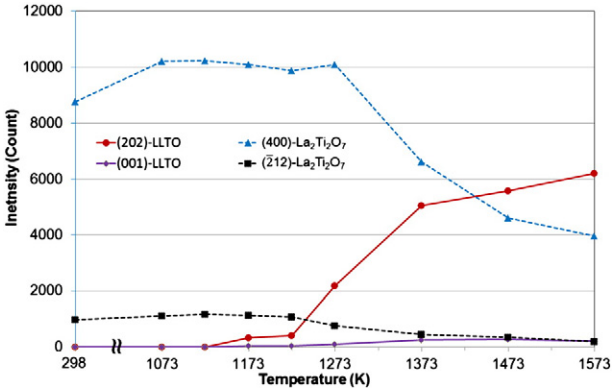

Fig. 3. Comparative intensity changes of the selected crystallographic planes related with the $La_2Ti_2O_7$ reactive template and the LLTO product phases.

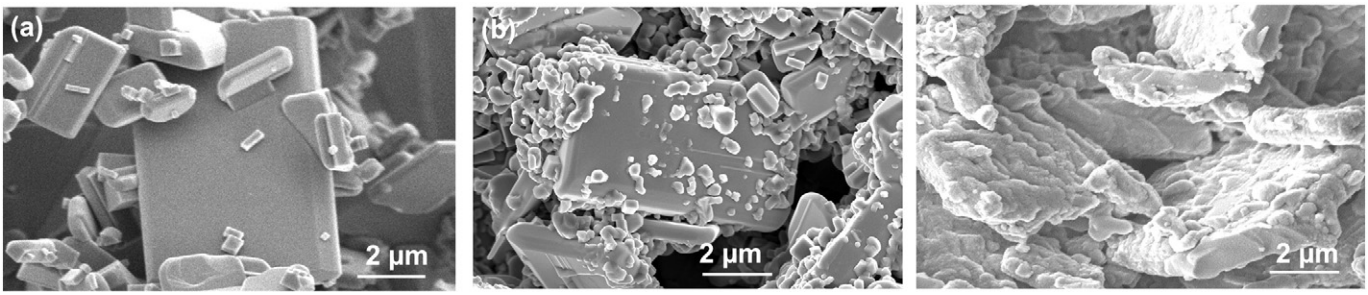

Fig. 4. SEM images of (a) the surfaces of the original $La_2Ti_2O_7$ template and the fracture surfaces of the heat-treated specimen at (b) 1173 and (c) 1273 K for 15 min.

condition where the interfaces analyzed were edge-on. However, this could be achieved by tilting the template grains to the [010] zone-axis. Because of this strong diffraction condition, systematic errors in EDS measurements due to channeling are very likely. Therefore, rather than the absolute values of La/Ti ratio, relative variations from column to column are more meaningful to discuss. The EDS measurements were taken from regions where the specimen thickness was between 0.4 and 1.0 times the mean free path. This was the best compromise between the signal amount, beam broadening effects, beam damage, and specimen drift. The atomic-plane-resolved EDS measurements were made in scanning mode with a window size of 0.4 nm × 4 nm. This allowed the simultaneous measurement and image viewing. The atomic-plane-thick and several-nanometer-long window allowed also averaging of column-to-column variation of the La/Ti ratio, especially in the La-poor planes close to the reaction interface. For each measurement, the measurement window was placed on the (001)-type planes of LLTO (La-rich or La-poor (001) planes).

3. Results

Fig. 2(a) shows XRD patterns obtained at different temperatures from the surface of a dewaxed body parallel to the tape-casting plane. Reference XRD data for the $La_2Ti_2O_7$ reactive template and LLTO product are shown in Fig. 2(b). No intermediate phase that could disturb the succession of the texture is observed in Fig. 2(a). The intensities of the $(\bar{2}12)$ and (400) $La_2Ti_2O_7$ peaks and the (202) and (100) LLTO peaks are plotted as a function of temperature in Fig. 3. As stated before, the template $La_2Ti_2O_7$ particles showed a faceted morphology parallel to {*h*00} in our recent study [14]. Thus, the {*h*00} planes are aligned parallel to the sheet surface, owing to the shear stress during tape casting. Therefore, the intensity of the (400) peak is expected to be strong for the sheet surface, as compared with that for the $(\bar{2}12)$ $La_2Ti_2O_7$ peak (the strongest in the reference data in Fig. 2(b)). The increase in the intensity of the (202) LLTO peak is attributed to the formation of the LLTO phase and the development of $(110)_{pc}$ texture [22]. In Fig. 3, the LLTO phase appears at 1173 K with a low diffraction intensity, although the (202) LLTO peak cannot be detected clearly in Fig. 2(a). However, the intensity of the (202) LLTO peak increases significantly at 1273 K, while that of the (400) $La_2Ti_2O_7$ peak diminishes dramatically. Thus, it can be concluded that the conversion of $La_2Ti_2O_7$ into LLTO had already started at 1173 K.

Fig. 4(a) shows an SEM image of the surface of the reactive templates. Fig. 4(b) and (c) show SEM fractographs of specimens heat-treated for 15 min at 1173 and 1273 K, respectively. Following heat treatment at 1173 K, no distinct change is observed on the template surfaces compared with the original reactive template particles. However, a clear morphological change is observed on the template surfaces heat-treated at 1273 K, in that submicron-scale undulated structures are seen to be present. This specimen was selected for TEM analysis, since both the HTXRD and SEM results clearly indicated the formation of an LLTO phase.

A low-magnification TEM image of the two-phase boundary region of the specimen heat-treated at 1273 K is shown in Fig. 5(a). Fig. 5(b) and (c) show SAED patterns obtained from the reactive template and the product, respectively. The pattern in Fig. 5(c) corresponds to a layered structure, indexed as monoclinic $La_2Ti_2O_7$ viewed along the [010]

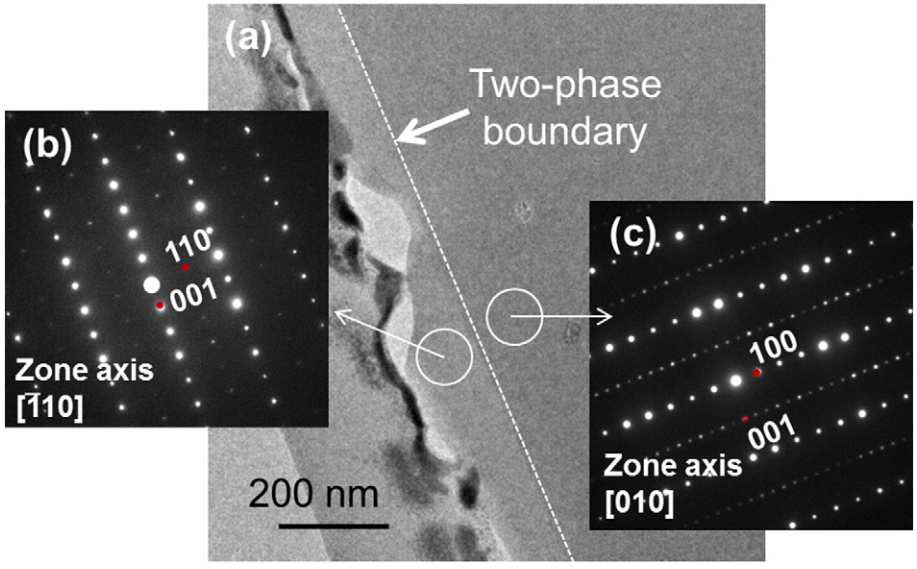

Fig. 5. (a) Low-magnification TEM image of the two-phase boundary region of the specimen heat-treated at 1273 K for 15 min, and SAED patterns corresponding to (b) the regular-perovskite product and (c) the $La_2Ti_2O_7$ reactive template.

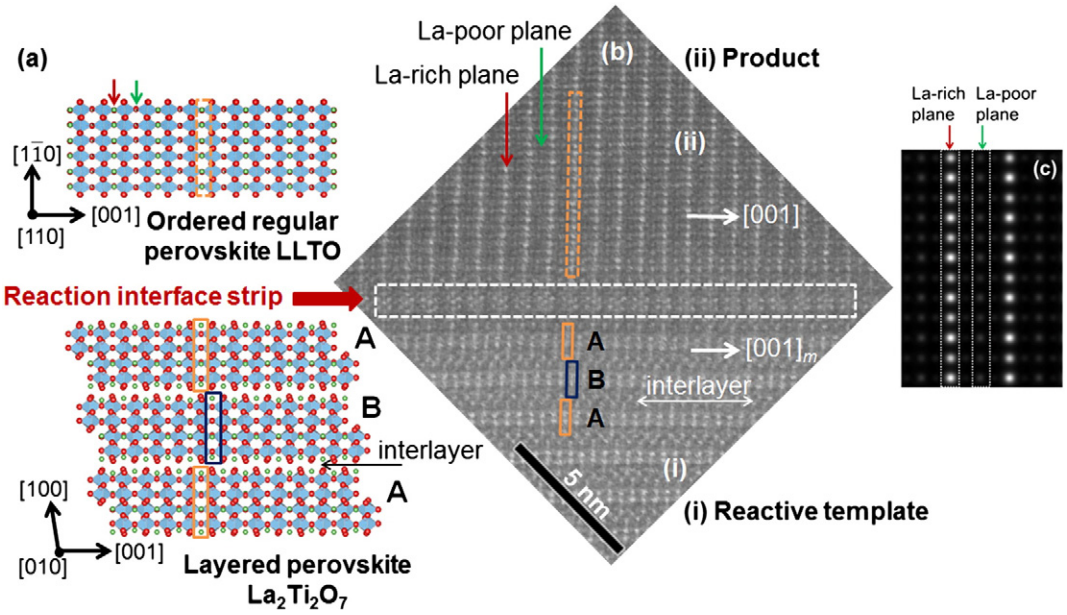

Fig. 6. (a) Crystallographic relationship between the template and the product across the reaction interface. (b) HAADF image of the two-phase boundary of the specimen heat-treated at 1273 K for 15 min. The upper part of the image, ii, corresponds to the LLTO product phase with periodic La-rich and La-poor planes along the [001] direction and the lower part of the image, i, corresponds to the $La_2Ti_2O_7$ reactive template. The white-dashed area on the HAADF image shows the reaction-interface strip formed during the topochemical conversion from $La_2Ti_2O_7$ to LLTO. A and B are thin blocks containing four layers of TiO_6 octahedra between two interlayers in the $La_2Ti_2O_7$ crystal structure. (c) Simulated-HAADF image of the LLTO structure along the [110] zone axis.

zone axis. The pattern in Fig. 5(b) is indexed as an orthorhombic crystal structure viewed along the [$\bar{1}$10] zone axis. However, on the basis of the unit cell for $Li_{0.16}La_{0.62}TiO_3$ ($a = 7.745$ Å, $b = 7.722$ Å, $c = 7.773$ Å [22]), the structure is hereafter assumed to be a pseudocubic regular perovskite for simplicity. It was found that the interface lay parallel to the {100} $La_2Ti_2O_7$ reactive template and the $\{110\}_{pc}$ regular perovskite product.

An HAADF image of the two-phase boundary is shown in Fig. 6(b). The upper part of the image, ii, corresponds to the product phase, while the lower part, i, corresponds to the $La_2Ti_2O_7$ reactive template. The brightest spots in the image are attributed to La columns with a high atomic number ($Z = 57$). In a thin block of the $La_2Ti_2O_7$ structure containing four layers of TiO_6 octahedra, La atoms are positioned in a plane that lies normal to the interlayer (colored rectangles in Fig. 6(a)). The positions of the La atoms are shifted along the *c*-axis by ~2 Å (a quarter of the lattice parameter) with respect to those in the vertically adjacent blocks in $La_2Ti_2O_7$. The upper part of the image, ii, shows alternating La-rich (red arrow) and La-poor planes (green arrow), which exhibit brighter and dimmer contrast, respectively, because of their different La occupancy values [9]. Ordering of the (001)-type planes into La-rich or La-poor planes was confirmed by the different La/Ti atomic ratios estimated from the EDS measurements performed on the (001)-type La-rich or La-poor planes. The average values with standard deviations of La/Ti atomic ratios were 0.74 ± 0.06 and 0.63 ± 0.10 for the bright and dim columns determined from 6 to 10 EDS measurements, respectively. The precision of the absolute La/Ti ratio for each individual EDS measurement is much worse due to possible channeling effects than the error bars reported here. The reported error bars are calculated from the variations between the measurements of individual La-poor or La-rich planes. We confirmed that the newly formed LLTO phase in the FIB-prepared TEM specimen did show a single-domain structure without 90° domain boundaries, with a width of ~100 nm all the way to the surface from two-phase boundary along ~1 μm length. However, the presence or location of Li atoms could not be determined by this analysis. The HAADF image of the $Li_{0.16}La_{0.62}TiO_3$ crystal along the [110] zone axis was simulated using the Quantitative Scanning Transmission Electron Microscope (QSTEM) software package [23] with our microscope parameters. The QSTEM image in Fig. 6(c) also shows a structure with alternating La-rich and La-poor planes. A reaction-interface "strip" (white-dashed rectangle) is observed along the two-phase boundary in Fig. 6(b). Since the reaction strip was sensitive to electron beam and damaged easily, any quantitative analysis based on composition and atomic distribution of the reaction strip could not yet be attained.

In Fig. 7, the structural transition of the reaction strip can be monitored clearly from the right side to the left in a high-magnification

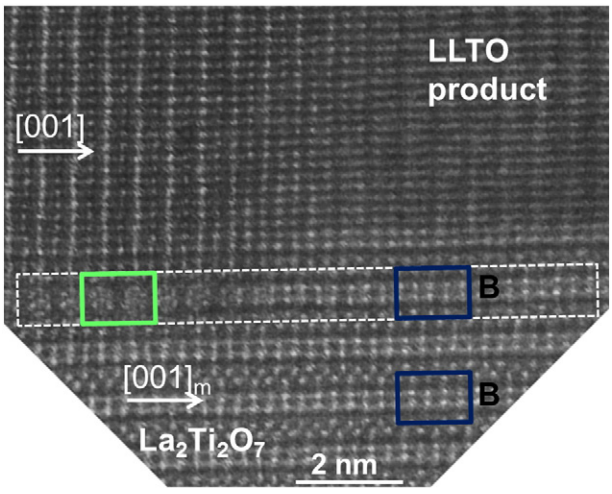

Fig. 7. High-magnification HAADF image of the two-phase boundary of the specimen heat-treated at 1273 K for 15 min. White-dashed area indicates the reaction strip formed during the topochemical conversion at the interface. The right side of the reaction strip (blue-colored frame) exhibits the same La-atom arrangement of block B (Fig. 6) in the $La_2Ti_2O_7$ structure. The left side of the reaction strip (green-colored frame) shows the transient structure from "block B" $La_2Ti_2O_7$ in the course of the rearrangement of La-atoms during conversion reaction.

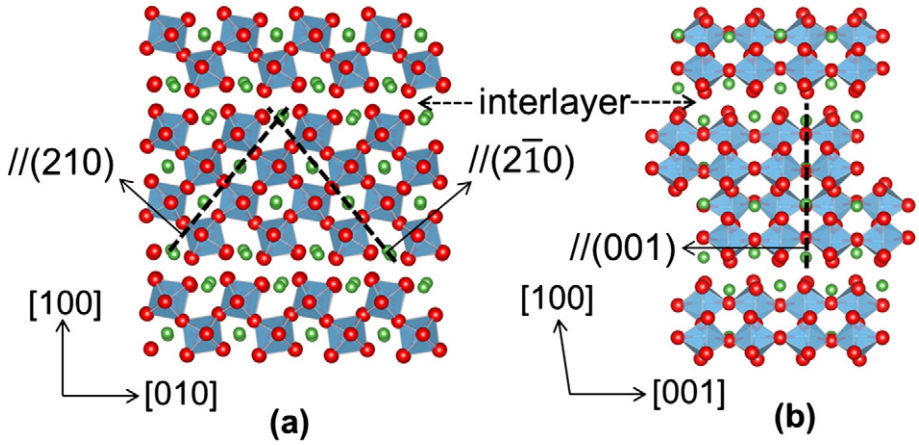

Fig. 8. Configurations of (a) (210), (2$\bar{1}$0) and (b) (001) planes in the $La_2Ti_2O_7$ crystal structure [8].

HAADF image. The structure of $La_2Ti_2O_7$ (blue–colored frame) is converted gradually into a transient state (green-colored frame) along the $[001]_m$ direction. Accordingly, the interface strip revealed a unit-cell-thick $La_2Ti_2O_7$ reactive template. In addition, the thickness of the reaction strip was measured to be ~1.3 nm in Fig. 7. This result is in a good agreement with the height of the $La_2Ti_2O_7$ unit-cell (1.286 nm). Thus, it can be concluded that a regular perovskite-type product exists, with alternating La-rich and La-poor planes oriented perpendicular to the reaction interface. The topochemical conversion mechanism at play in this system will be discussed in Section 4.

4. Discussion

A reaction-interface strip with a thickness of the $La_2Ti_2O_7$ unit-cell is observed in Fig. 6(b). When viewed along the *b*-axis, the crystal structure of $La_2Ti_2O_7$ consists of alternating stacks of two types of thin blocks vertically separated by an interlayer and horizontally displaced by a quarter of the lattice parameter along the *c*-axis, as illustrated in Fig. 6(a). Each thin block is composed of four layers of corner-sharing TiO_6 octahedra between two interlayers. These blocks are crystallographically similar to the regular perovskite structure, and Ti and O are known to form strong periodic Ti–O bond chains. Therefore, it is proposed that the blocks of four-layered TiO_6 octahedra in $La_2Ti_2O_7$ can rearrange their positions with slight shifts along the *c*-axis, while preserving their Ti–O bonding and alignment during the conversion reaction. The STEM image indicates that one of the two types of blocks (A) in the $La_2Ti_2O_7$ reactive template has La atoms on the same vertical lines as those in the LLTO product, whereas the other (B) has La positions displaced in the *c*-direction. Thus, upon conversion from template to product, block A retains its relative position, while block B shifts by ~2 Å along the *c*-axis. This shift is accompanied by the rearrangement and out-diffusion of La atoms. It appears that the reaction-interface strip in the STEM image is the transient stage of block B, with La atoms shifting during the conversion. A high-magnification HAADF image (Fig. 7) clearly shows the transition from the conserved "block B" $La_2Ti_2O_7$ (blue-colored frame) to the transient structure (green-colored frame) in the reaction strip at the interface. The topochemical conversion must proceed with unit-cell-thick TiO_6 octahedron blocks in the layered-perovskite phase to be transformed into the regular-perovskite phase in a layer-by-layer manner.

When we consider the topochemical relationship between the crystal structures of $La_2Ti_2O_7$ and LLTO, there are three possible configurations for the La-rich and La-poor planes in the LLTO product: (i) parallel to (001), and almost parallel to (ii) (210) and (iii) (2$\bar{1}$0) in $La_2Ti_2O_7$. The configurations of the (001), (210) and (2$\bar{1}$0) planes in the $La_2Ti_2O_7$ crystal structure are illustrated in Fig. 8 [8]. However, we only observed the ordered planes in the product phase parallel to the (001) plane in $La_2Ti_2O_7$. This might be because the macroscopic direction of out-diffusing La and in-diffusing Li is parallel to (001) in $La_2Ti_2O_7$. When the chemistry of La-rich or La-poor (001)-type planes were analyzed, it was observed that the chemistry of the La-poor planes revealed a stronger statistical variation towards the reaction/conversion front. The La/Ti ratio values reported are already averaged over several atomic columns as the measurements were done by scanning over the (001)-type plane with a window size of atomic column width (~0.4 nm) and several tens of atomic column length (4.0 nm). This allowed the averaging of column-to-column variation in the La/Ti ratio along one (001)-type La-poor plane. Even then the La/Ti ratio varied more than that along La-rich planes. This stronger variation in the La/Ti ratio along La-poor (001)-type planes are most likely indicative of that these planes are taking an active role in the transportation of La-ions away from the reaction front towards the product phase, and the inward transportation of Li-ions towards the reaction front. However, the exact mechanism for producing this preferred configuration is yet not clear. The discovery of the uni-directionally ordered structure in the topochemically converted LLTO might aid the design and fabrication of domain-oriented polycrystals.

5. Conclusion

The reaction interface between a $La_2Ti_2O_7$ reactive template and an LLTO product was observed by TEM and found to be parallel to the interlayers, i.e., the (200) planes of the $La_2Ti_2O_7$ template. The crystallographic relationship between the two phases was determined to be orthorhombic LLTO [001](110) || monoclinic $La_2Ti_2O_7$ [001](100). Blocks of four-layered TiO_6 octahedra between two interlayers in $La_2Ti_2O_7$ are thought to be the basic units for topochemical conversion to a regular perovskite-type product. Alternating La-rich and La-poor planes in the LLTO phase were aligned perpendicular to the interface and parallel to the {001} plane in $La_2Ti_2O_7$. These microscopy observations of the well-aligned interface and ordered structure suggest the possibility of designing domain-oriented microstructure with improved ionic conductivity.

Acknowledgements

The authors would like to thank Messrs. Y. Kishida and T. Uyama, Mses. Tamano Miura and Kazumi Tanaka of Toyota Central Research and Development Laboratories, Inc. as well as Mr. Turgay Gonul of Sabanci University for their technical supports including HTXRD analysis, specimen preparation and microscopy. Discussions with Mr. Hidehito Matsuo and Dr. Shigeo Hori of Toyota Central Research and Development Laboratories, Inc. are also greatly acknowledged. This work is

supported by the collaborative PhD program of Toyota Technological Institute and Toyota Central Research and Development Laboratories, Inc. with the funding of Toyota Scholarship Foundation.

References

[1] B. Scrosati, J. Garche, J. Power Sources 195 (2010) 2419–2430.
[2] P.G. Balakrishnan, R. Ramesh, T. Prem Kumar, J. Power Sources 155 (2006) 401–414.
[3] S. Stramare, V. Thangadurai, W. Weppner, Chem. Mater. 15 (2003) 3974–3990.
[4] Y. Inaguma, L.Q. Chen, M. Itoh, T. Nakamura, T. Uchida, H. Ikuta, M. Wakihara, Solid State Commun. 86 (1993) 689–693.
[5] Y. Inaguma, J.D. Yu, T. Katsumata, M. Itoh, J. Ceram. Soc. Jpn. 105 (1997) 548–550.
[6] O. Bohnke, Solid State Ionics 179 (2008) 9–15.
[7] X. Gao, C.A.J. Fisher, T. Kimura, Y.H. Ikuhara, H. Moriwake, A. Kuwabara, H. Oki, T. Tojigamori, R. Huang, Y. Ikuhara, Chem. Mater. 25 (2013) 1607–1614.
[8] K. Momma, F. Izumi, J. Appl. Crystallogr. 44 (2011) 1272–1276.
[9] Y. Inaguma, T. Katsumata, M. Itoh, Y. Morii, J. Solid State Chem. 166 (2002) 67–72.
[10] M. Yashima, M. Itoh, Y. Inaguma, Y. Morii, J. Am. Chem. Soc. 127 (2005) 3491–3495.
[11] X. Gao, C.A.J. Fisher, T. Kimura, Y.H. Ikuhara, A. Kuwabara, H. Moriwake, H. Oki, T. Tojigamori, K. Kohamac, J. Mater. Chem. A 2 (2014) 843–852.
[12] Y. Inaguma, T. Katsumata, M. Itoh, Y. Morii, T. Tsurui, Solid State Ionics 177 (2006) 3037–3044.
[13] H. Moriwake, X. Gao, A. Kuwabara, C.A.J. Fisher, T. Kimura, Y.H. Ikuhara, K. Komaha, T. Tojigomori, Y. Ikuhara, J. Power Sources 276 (2015) 203–207.
[14] K. Takatori, K. Saura, A. Orum, H. Kadoura, T. Tani, J. Eur. Ceram. Soc. 36 (2016) 551–558.
[15] T. Tani, J. Ceram. Soc. Jpn. 114 (2006) 363–370.
[16] PDF#00-028-0517, Natl. Bur. Stand. U.S. Monogr. 25-15 (1978) 35.
[17] M. Hojamberdiev, A. Yamaguchi, K. Yubuta, S. Oishi, K. Teshima, Inorg. Chem. 54 (2015) 3237–3244.
[18] A. Orum, K. Takatori, S. Hori, T. Ikeda, M. Yoshimura, T. Tani, Jpn. J. Appl. Phys. 55 (2016), 08NB08.
[19] T. Takeuchi, T. Tani, J. Ceram. Soc. Jpn. 110 (2002) 232–236.
[20] Y. Seno, T. Tani, Ferroelectrics 224 (1999) 365–372.
[21] T. Watanabe, M. Watanabe, T. Suziki, S. Yamabi, H. Yabuta, K. Miura, N. Ito, N. Kumada, Jpn. J. Appl. Phys. 53 (2014), 09PB08.
[22] PDF#01–073-9131, Calculated from ICSD using POWD-12++ (2008).
[23] C. Koch, Determination of Core Structure Periodicity and Point Defect Density Along Dislocations, 2002 PhD thesis.